In-situ TEM annealing of amorphous Fe-24at.%W coatings and the effect of crystallization on hardness

(article starts on next page)

Metals & corrosion

In-situ TEM annealing of amorphous Fe-24at.%W coatings and the effect of crystallization on hardness

Antonio Mulone[1,*] 🔟, Inga Ennen[2], Andreas Hütten[2], and Uta Klement[1]

[1] *Department of Industrial and Materials Science, Chalmers University of Technology, SE-412 96 Gothenburg, Sweden*
[2] *Faculty of Physics, Center for Spinelectronic Materials and Devices, Bielefeld University, 33615 Bielefeld, Germany*

ABSTRACT

This paper describes the crystallization which occurs upon annealing of an amorphous Fe-24at.%W coatings, electrodeposited from a glycolate-citrate plating bath. A combination of Differential Scanning Calorimetry and in-situ Transmission Electron Microscopy annealing is used to study the onset of crystallization of the amorphous coating. The in-situ TEM analyses reveal the formation of first crystallites after annealing at 400 °C for 30 min. Upon a temperature increase to 500–600 °C, the crystallites develop into Fe-rich nanocrystals with $\sim$ 40 nm grain size. The nanocrystals are dispersed in the remaining amorphous Fe-W matrix, which results in the formation of a mixed nanocrystalline-amorphous structure. The observed crystallization can be held responsible for the increase in the hardness obtained upon annealing of Fe-24at.%W coatings. In fact, the hardness of the as-deposited material increases from 11 to 13 GPa after annealing at 400 °C, and it reaches the maximum value of 16.5 GPa after annealing at 600 °C.

Introduction

Lately, electrodeposited Fe-based alloys have gained considerable attention as a sustainable alternative to coatings produced using environmentally hazardous processes such as hard chrome coatings [1–3]. Because of the excellent properties such as high hardness and high wear and corrosion resistance, hard chromium coatings are commonly applied in aerospace and automotive applications, among others [4]. Yet, the deposition of such coatings requires the use of toxic and cancerogenic compounds such as Cr^{6+} [5]. In contrast, Fe-W alloys can be electrodeposited from environmentally friendly and thermodynamically stable electrolytes [6]. By properly varying the electrodeposition parameters (i.e., pH, temperature and current density) such coatings can be deposited with tuneable composition and microstructure [7]. In particular, the co-deposition of W has shown to strongly influence the microstructure of the Fe-W coatings resulting in a

transition from a nanocrystalline to a homogeneous amorphous structure when increasing the amount of deposited W [8]. As a result of the W-induced amorphization, Fe-W alloys containing high amounts of W (here: 24 at.% of W) are characterized with high hardness, $\sim$ 11 GPa [7]. The obtained as-deposited hardness is comparable to the hardness of hard Cr-coatings and exceeds the hardness of other W-containing electrodeposited coatings, e.g., Co- and Ni-based alloys [7, 9]. Furthermore, the hardness of Fe-W coatings can even be increased by heat treatments. In a previous work, Mulone et al. [10] investigated the effect of heat treatments on microstructure and mechanical properties of Fe-W coatings electrodeposited with various W contents. The authors observed that the hardness of Fe-24at.%W coatings was significantly increasing after annealing treatment at 400 °C, and it was reaching a maximum of 16.5 GPa upon annealing at 600 °C. The maximum in the hardness was related to the partial crystallization of the Fe-24at%W coatings with the formation of α-Fe crystalline phase when annealing at 600 °C, as revealed by XRD analysis [10]. However, XRD analyses did not reveal any microstructural transformation in the Fe-W coatings that could explain the substantial increase in the hardness (about 20%) obtained already at 400 °C. Several studies have shown how in-situ heating analyses can help in obtaining useful information on the crystallization mechanism of amorphous electrodeposited alloys [11, 12]. Hence, in this work in-situ Transmission Electron Microscopy (TEM) annealing experiments are performed with the aim to monitor the microstructural transformation occurring when annealing amorphous Fe-24at.%W coatings and to explain the increase in the hardness obtained after annealing at temperatures above 400 °C.

Materials and methods

Electrodeposition of Fe-W coatings

The Fe-W coatings were electrodeposited from a Fe(III)-based glycolate-citrate electrolyte, and the deposition parameters were applied to obtain a Fe-W coating with 24 at.% of W. Details about the electrodeposition can be found in [7]. For the deposition of the samples, a three-electrode cell was used composed of (1) a copper sheet as working electrode, a (2) platinized titanium was used as a counter electrode and (3) a saturated Ag/AgCl/KCl reference electrode. Prior to performing Differential Scanning Calorimetry (DSC) and TEM analysis, the Fe-24at.%W coating was mechanically removed (stripped off) from the substrate.

Characterization of Fe-W coatings

X-rays diffraction (XRD) spectra of the as-deposited and heat-treated Fe-24at.%W coatings were acquired using a Bruker AXS D8 advance diffractometer with Cr Kα radiation (λ = 2.28970 Å) which was operated at 40 kV and 50 mA. Prior to XRD analysis, the Fe-24at.%W coatings were annealed under argon atmosphere in the furnace of a NETZSCH 402 C dilatometer. The samples were kept for one hour at 400, 600 and 800 °C and afterward were cooled down to room temperature inside the furnace. The DSC measurement was performed using a thermal analyzer STA 449 F1 Jupiter from NETZSCH. The sample was loaded in PtRh/Al_2O_3 crucibles and heated up to 800 °C with a heating rate of 10 °C /min under argon atmosphere. Two successive heating scans were performed in order to capture the irreversible transformations occurring upon annealing. In-situ TEM analyses were conducted in a JEOL JEM 2200FS which was operated at 200 keV. The annealing was performed using a specimen heating-tilting holder from JEOL. In the TEM, the samples were annealed successively at 300, 400, 500 and 600 °C for 30 min. EDS analyses were performed on the annealed samples using a TEM FEI Titan 80–300 which was operated at 300 keV. Processing and standardless quantification of EDS data was performed using the TIA (TEM Imaging and Analysis) software. The background was removed from the spectra through a digital filtering algorithm, whereby the background is convoluted with a "top-hat" filter. Using a standardless quantification procedure, the peaks are then fitted to theoretical Gaussian peaks and the integrated peak intensity is calculated. Finally, the integrated intensity is used together with the Cliff-Lorimer k-factors and a thin-foil absorption correction to calculate the elemental composition. For the TEM analyses, disk-shaped specimens were punched out from a substrate-free Fe-24at.%W sample. Each disk-shaped specimen was ion milled in a Gatan precision ion polishing system using a beam energy of 5 keV and 6° and 3° as angles of incidence,

respectively. Investigations by electron back scatter diffraction (EBSD) technique were performed using a Leo 1550 Gemini Scanning Electron Microscope (SEM) with field emission gun which was equipped with a Nordlys II detector (Oxford Instruments). The EBSD phase map was acquired from the cross section of the Fe-24at.%W coating after annealing at 800 °C. EBSD data were post-processed using HKL Channel 5 software (Oxford Instruments): noise reduction was done by removal of wild spikes and extrapolation of non-indexed points (5 nearest neighbors required).

Results and discussion

Figure 1 shows the Fe-24at.%W X-ray diffraction profiles in the as-deposited condition and after annealing at 400 °C, 600 °C and 800 °C in Ar atmosphere. The insert included in Fig. 1 shows the hardness evolution of the coatings after annealing. The hardness was measured using a nanoindentation tester, the measurements are described in details in our previous study [10]. The structure of the as-deposited Fe-24at.%W coating is amorphous, as can be observed from the broad shoulder starting at $2\theta \sim 60°$ in the XRD spectrum in Fig. 1. Despite the increase in the hardness after annealing at 400 °C, the XRD results do not reveal any evidence for the occurrence of crystallization since the XRD diffraction profiles of the annealed and the as-deposited samples are identical (see Fig. 1). The main
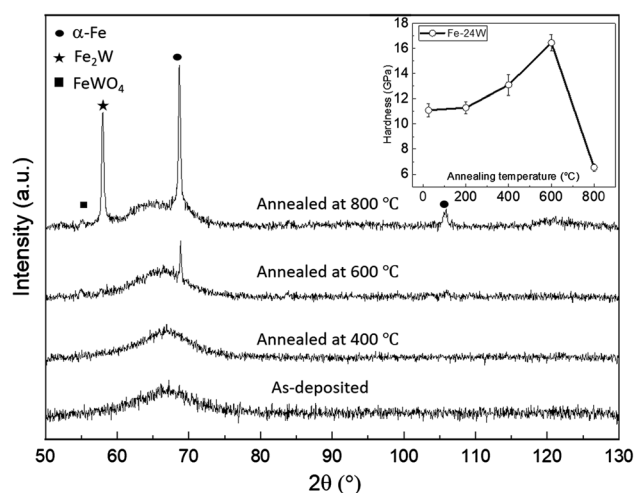
crystallographic transformations are observed after annealing at 600 °C with the formation of α-Fe phase, and after annealing at 800 °C with the formation of Fe_2W and $FeWO_4$. The formation of the $FeWO_4$ phase is thought to be favored by oxygen contamination in the Ar atmosphere. In fact, the formation of the $FeWO_4$ phase is mainly observed at the surface of the annealed Fe-24at.%W coatings [2]. Furthermore, the $FeWO_4$ phase is not observed when performing the annealing in vacuum [8].

DSC analysis was performed on the Fe-24at.%W coatings to gather further information regarding the onset temperature of crystallization upon annealing. The DSC curve, shown in Fig. 2, is characterized by a broad exotherm and 2 overlapping peaks. The broad exotherm has its onset at ~ 250 °C. The first exothermic peak has an onset temperature (T_o) at 600 °C and a maximum at 670 °C (T_p). The second peak is overlapping with the first exothermic peak and occurs at ~ 740 °C. In connection with the XRD results shown in Fig. 1, the broad exotherm can be related to the formation of the α-Fe phase. The amount of the crystalized α-Fe increases with increasing the annealing temperature, resulting in the appearance of the α-Fe XRD peak after annealing at 600 °C for 1 h (see Fig. 1). Regarding the 2 exothermic peaks observed at higher temperature, the main peak at 670 °C can be related to the formation of the Fe_2W, while the peak at ~ 740 °C can be associated with the formation of the $FeWO_4$ phase.

Figure 1 X-ray diffraction patterns of as-deposited and annealed Fe-24at.%W coatings. The insert shows the hardness variation of the coatings upon annealing treatment.
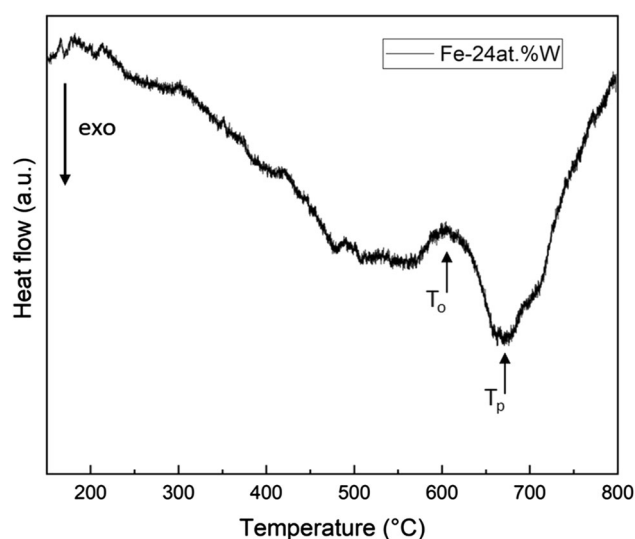

Figure 2 DSC curve acquired from the as-deposited Fe-24at.%W sample. Marked are the crystallization on-set temperature, T_o, and the peak temperature, T_p.

This reasoning is supported by the high fraction of Fe_2W phase formed. The intensities of the diffraction peaks of the XRD pattern can be related to the volume fraction of the different phases present in the material. As shown in Fig. 1, the intensity of the crystalline peak belonging to the Fe_2W phase is by far more prominent as compared to the intensity of the $FeWO_4$ peak.

To confirm the DSC results and the hypothesis regarding the broad exotherm observed in Fig. 2, in-situ TEM analyses were performed on the Fe-24at.%W coatings. As shown from the TEM results in Fig. 3, in the as-deposited state the electrodeposited Fe-24at.%W coatings have a homogenous amorphous structure. In fact, no diffraction spots are visible in the Fast Fourier Transform (FFT) acquired from the TEM micrograph shown in Fig. 3b.

As shown in Fig. 4a, after annealing at 300 °C for 30 min there are no visible changes in the amorphous structure of the Fe-24at.%W sample, i.e., the FFT shown in Fig. 4a is characterized with diffuse rings and no visible diffraction spots. The first microstructural transformations are visible after annealing for 30 min at 400 °C, see Fig. 4b. Annealing at this temperature leads to the formation of dispersed crystallites of ∼ 20 nm in diameter. The crystalline nature is confirmed by diffraction spots in the acquired FTT, see the inset in Fig. 4b. The formation of nanocrystals is more evident between 500 and 600 °C, as shown in Fig. 4c and d, respectively. The size of the nanocrystals has slightly increased, with an average crystallite size of 42 ± 20 nm (as averaged from the grain size of 10 different grains), and their number has increased substantially. To reveal the chemical composition of the formed nanocrystals, EDS point analysis was performed and the results are shown in Fig. 5. The composition of the nanocrystal and of the Fe-W matrix in Fig. 5 is presented as an average of 3 measurements acquired from different sites. As can be seen, the formed nanocrystals are rich in Fe (see Point 1 in Fig. 5c) as compared to the retained amorphous matrix (see Point 2 in Fig. 5c). The results suggest that the formed nanocrystals are α-Fe grains, as also observed from the XRD results in Fig. 1a. The observed crystallization phenomena can explain the increase in the hardness upon annealing Fe-24at.%W coatings above 400 °C. In fact, the hardness increase obtained already at 400 °C can be related to the formation of the first nanocrystals as seen in Fig. 4b. The in-situ TEM results also confirm the assumption that the broad DSC exotherm is related to the formation of α-Fe nanocrystals. The amount of nanocrystals formed below 600 °C seems to be just below the XRD detection limit of a few weight percent of the crystalline phase [13], and thus it does not appear in the XRD pattern in Fig. 1. The maximum in the hardness measured after annealing at 600 °C (see Fig. 1) is related to the obtained mixed amorphous–nanocrystalline structure. This finding is supported by previous studies on the crystallization of Fe and Zr-based bulk metallic glasses. These studies showed that the precipitation of nanocrystallites within an amorphous matrix can lead to a significant increase in hardness and Young´s modulus of the material [14, 15].

The decrease in the hardness observed after annealing above 600 °C is related to the grain growth of the α-Fe crystalline phase [10]. Such increase in the average α-Fe grain size can be observed from EBSD

Figure 3 a and **b** TEM micrographs of the amorphous as-deposited Fe-24at.%W sample. The micrograph shown in **b** is acquired with a higher magnification and includes the FTT acquired from the same area as inset.
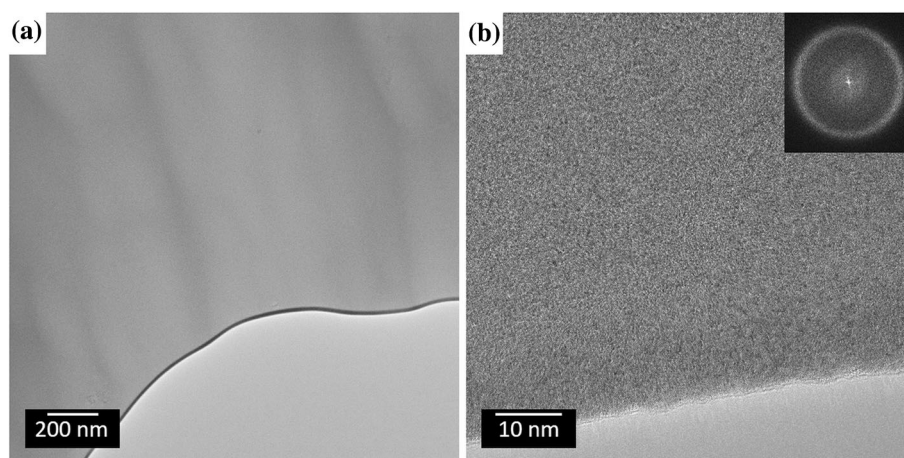
Figure 4 TEM micrographs after 30 min annealing at 300 °C **a**, 400 °C **b**, 500 °C **c** and 600 °C **d**. The boxes are showing the area where the FFTs were acquired.
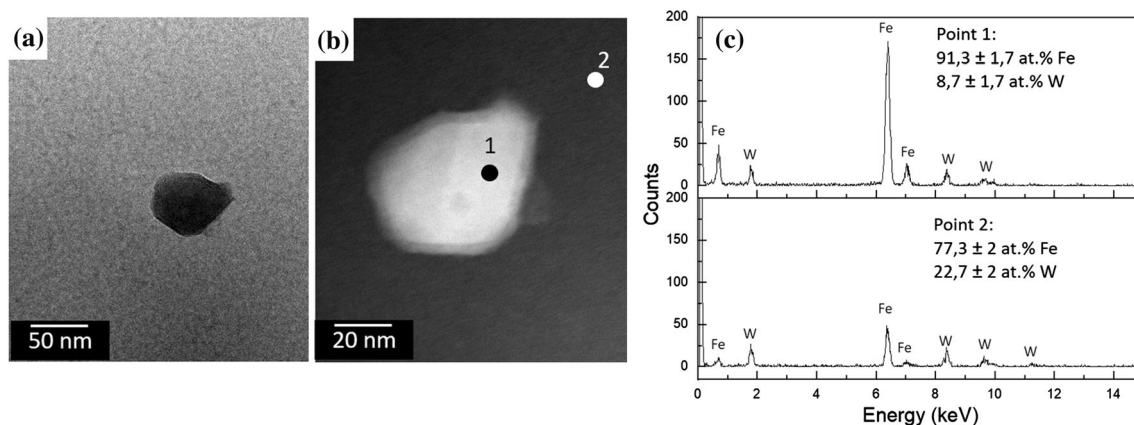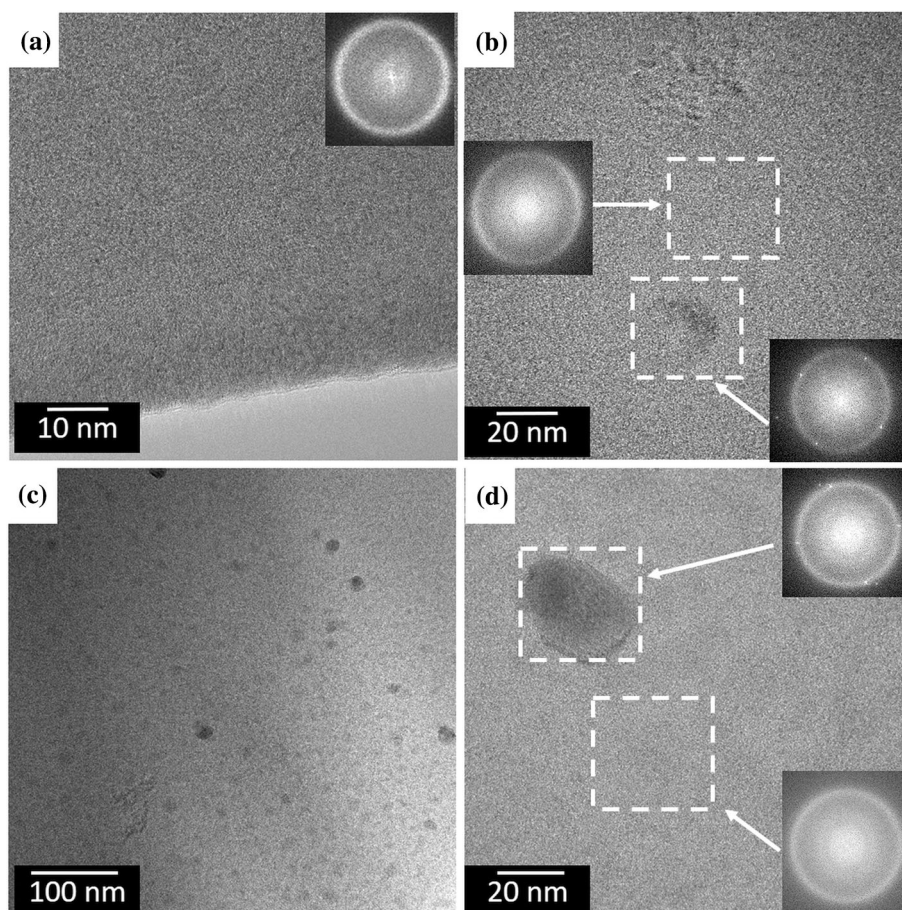

Figure 5 TEM micrographs acquired in bright field **a** and dark field **b** mode from the Fe-24at.%W sample annealed at 500 °C. Locations of EDS point analyses (given in **c**) are shown in the dark field image in **b**.

results shown in Fig. 6. The box in the in the SEM micrograph (Fig. 6a) marks the area where the phase map was acquired on the cross section of a Fe-24at.%W sample after annealing in Ar atmosphere for 1 h at 800 °C. The blue grains in the phase map belong to the α-Fe phase, while the violet grains belong to the Fe_2W phase. A large fraction of zero solutions is present, which appear as white pixels. Such high fraction (~ 50%) of zero solutions can be related to the amorphous phase which is retained after the heat treatment at 800 °C [2] which cannot be indexed by EBSD technique. XRD results acquired

Figure 6 Back scattered electron image of the cross section of the Fe-24at.%W sample annealed at 800 °C for 1 h **a**, EBSD phase map **b** and α-Fe grain size histogram **c**. The phase map is acquired from the white dashed box highlighted in **a**. In the phase map, the blue grains belong to α-Fe phase, while the violet grains are related to Fe_2W phase.
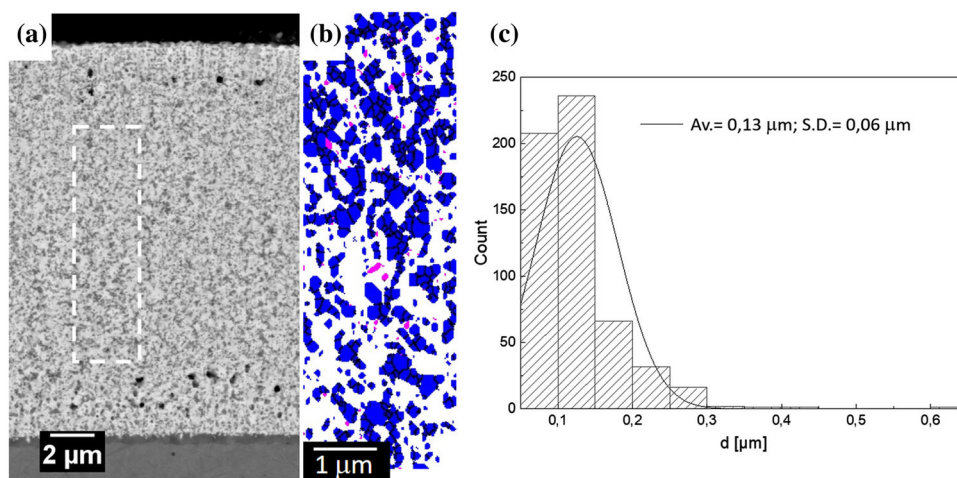
with grazing incidence geometry from a Fe-24at.%W sample annealed at 800 °C revealed that Fe_2W is mostly formed in the proximity of the sample surface [2], which explains the low fraction of Fe_2W phase included in the phase map ($\sim$ 3%) shown in Fig. 6. In Fig. 6c, the grain size histogram of the α-Fe grains is shown as measured from the EBSD phase map. The majority of α-Fe grains are between 100 and 150 nm in diameter, providing an average grain size of 130 $\pm$ 60 nm. The grain size is likely underestimated due to the large fraction of zero solutions, but the observed increase in grain size from $\sim$ 40 at 600 °C to $\sim$ 130 nm at 800 °C can be considered as the main reason for of the drop in hardness of the Fe-24at.%W coatings. A similar decrease in the hardness with increasing grain size has been observed in Ni-W coatings [16]. Here, a $\sim$ 40% decrease in the hardness is obtained when the grain size of Ni-W increase from $\sim$ 20 to over 100 nm.

Summary and conclusions

In this work the crystallization upon annealing of amorphous electrodeposited Fe-24at.%W coatings was studied with XRD, DSC, EBSD and (in-situ) TEM analysis. After 30 min annealing at 400 °C, in-situ TEM analysis revealed the formation of α-Fe nanocrystals of about 20 nm in diameter within the Fe-W amorphous matrix. When annealing up to 500 °C and 600 °C, the α-Fe nanocrystals grow in number and size, i.e., $\sim$ 40 nm in diameter. The formation of a mixed nanocrystalline–amorphous structure is held responsible for the substantial

increase in hardness, i.e., 16.5 GPa, which amounts to a 50% increase as compared to the hardness in the as-deposited state. As revealed by EBSD analysis, when annealing above 600 °C a higher amount α-Fe grains is formed and their grain size increases reaching an average value of $\sim$ 130 nm at 800 °C. The observed grain growth is causing a substantial decrease in the hardness of the Fe-24at.%W samples.

Compliance with ethical standards

Conflicts of interest No conflict of interest exists.

References

[1] Mulone A, Hildenbrand J, Klement U (2020) Electrodeposition: three steps towards sustainability. Trans Inst Met Finish 98:108–113

[2] Mulone A, Nicolenco A, Imaz N, Martinez-Nogues V, Tsyntsaru N, Cesiulis H, Klement U (2019) Improvement in the wear resistance under dry friction of electrodeposited Fe–W coatings through heat treatments. Coatings 9:66

[3] Mulone A, Nicolenco A, Imaz N, Fornel J, Sort J, Klement U (2020) Effect of heat treatments on the mechanical and tribological properties of electrodeposited Fe–W/Al2O3 composites. Wear 448–449:203232

[4] Lausmann GA (1996) Electrolytically deposited hard-chrome. Surf Coat Technol 86–87:814–820

[5] Baral A, Engelken R, Stephens W, Farris J, Hannigan R (2006) Evaluation of aquatic toxicities of chromium and chromium-containing effluents in reference to chromium electroplating industries. Arch Environ ContamToxicol 50:496–502

[6] Nicolenco A, Tsyntsaru N, Cesiulis H (2017) Fe (III)-based ammonia-free bath for electrodeposition of Fe-W Alloys. J ElectrochemSoc 164:D590–D596

[7] Nicolenco A, Tsyntsaru N, Fornell J, Pellicer E, Reklaitis J, Baltrunas D, Cesiulis H, Sort J (2018) Mapping of magnetic and mechanical properties of Fe-W alloys electrodeposited from Fe(III)-based glycolate-citrate bath. Mater Des 139:429–438

[8] Mulone A, Nicolenco A, Hoffmann V, Klement U, Tsyntsaru N, Cesiulis H (2018) In-depth characterization of as-deposited and annealed Fe-W coatings electrodeposited from glycolate-citrate plating bath. ElectrochimActa 261:167–177

[9] Tsyntsaru N, Cesiulis H, Donten M, Sort J, Pellicer E, Podlaha-Murphy EJ (2013) Modern trends in tungsten alloys electrodeposition with iron group metals. Surf EngAplElectrochem 48:491–520

[10] Mulone A, Nicolenco A, Fornell J, Pellicer E, Tsyntsaru N, Cesiulis H, Sort J, Klement U (2018) Enhanced mechanical properties and microstructural modifications in electrodeposited Fe-W alloys through controlled heat treatments. Surf Coat Technol 350:20–30

[11] Modin EB, Pustovalov EV, Fedorets AN, Dubinets AV, Grudin BN, Plotnikov VS, Grabchikov SS (2015) Atomic structure and crystallization processes of amorphous (Co, Ni)-P metallic alloy. J Alloys Compd 641:139–143

[12] Pustovalov EV, Modin EB, Voitenko OV, Fedorets AN, Dubinets AV, Grudin BN, Plotnikov VS, Grabchikov SS (2014) Structure relaxation and crystallization of the CoW-CoNiW-NiW electrodeposited alloys. Nanoscale Res Lett 9:1–8

[13] Newman JA, Schmitt PD, Toth SJ, Deng F, Zhang S, Simpson GJ (2015) Parts per million powder X-Ray diffraction. Anal Chem 87:10950–10955

[14] Fornell J, González S, Rossinyol E, Suriñach S, Baró MD, Louzguine-Luzgin DV, Perepezko JH, Sort J, Inoue A (2010) Enhanced mechanical properties due to structural changes induced by devitrification in Fe–Co–B–Si–Nb bulk metallic glass. Acta Mater 58:6256–6266

[15] Wang JG, Choi BW, Nieh TG, Liu CT (2000) Crystallization and nanoindentationbehavior of a bulk Zr–Al–Ti–Cu–Ni amorphous alloy. J Mater Res 15:798–807

[16] Trelewicz JR, Schuh CA (2007) The Hall-Petch breakdown in nanocrystalline metals: a crossover to glass-like deformation. Acta Mater 55:5948–5958